Journal of
Materials Chemistry A

Materials for energy and sustainability

Accepted Manuscript

This article can be cited before page numbers have been issued, to do this please use: Q. H. Al-Galiby, L. A. Algharagholy, H. Sadeghi and V. Garcia Suarez, *J. Mater. Chem. A*, 2025, DOI: 10.1039/D4TA08282F.

ROYAL SOCIETY OF CHEMISTRY

rsc.li/materials-a

View Article Online
DOI: 10.1039/D4TA08282F

Highly efficient thermoelectric converters based on metalloporphyrin nanotubes

Qusiy H. Al-Galiby[1*], Laith A. Algharagholy[2], Hatef Sadeghi[3] and Víctor M. García-Suárez[4*]

[1]Department of Physics, College of education, University of Al-Qadisiyah, Al Diwaniyah 58002, Iraq.
[2]Department of Physics, College of Science, University of Sumer, Al-Rifaee, 64005, Thi-Qar, Iraq.
[3]Device Modelling Group, School of Engineering, University of Warwick, Coventry CV47AL, UK.
[4]Departamento de Física, Universidad de Oviedo & CINN, Oviedo, 33007, Spain.
[*]Corresponding author: qusiy.algaliby@qu.edu.iq, vm.garcia@cinn.es

Abstract

Novel devices based on porphyrin nanotubes may lead to a wide range of uses in electronic functionality and thermoelectric conversion. π-conjugated metallo-porphyrin nanotubes have been designed with a configuration of opposite charged porphyrin molecules, which leads to oscillatory bandgaps as a function of the diameter of the nanotube. We focus in this work on bottom-up porphyrin nanotubes, rather different from conventional carbon nanotubes, which makes them also favorable candidates for making precursors of nanotube devices. We exploited the asymmetric band gap feature to design configurations of stacked six-metalloporphyrin rings connected by butadiyne to form periodic nanotube structure with different metallic atoms (Zn, Fe, and Fe-Cl). The electronic transport properties encapsulated in the transmission coefficients show that these porphyrin nanotubes in the presence of Zn give step-like features at asymmetric locations relative to the Fermi energy (E_F), which leads to huge enhancements of the thermoelectric performance. The highest values obtained for the thermopower, and the electronic figure of merit can also be obtained for many different positions of E_F, which makes Zn-porphyrin nanotube an optimal candidate for designing novel thermoelectric devices.

1. Introduction

The organization of metallo-porphyrin molecules in one-dimensional nanostructures, like for instance nanotubes, are of great interest for several properties that can incorporate: discrete π-conjugated electronic systems [1-7], tunable bandgaps [8] and quantum confinement effect in self-assembled binary porphyrin structures [9]. Such structures can have different forms, like for example stacked and cyclic nanorings of six butadiynes (C4)-linked porphyrin units (labeled *c*-P6) [10]. Notice that the use of other linkers (C0, C2), both along the circumference of the nanotube or along the nanotube axis is also possible; however, in the first case (circumference) the use of smaller linkers would cause additional tension that would make it necessary the use

View Article Online
DOI: 10.1039/D4TA08282F

of more porphyrin units along that direction; in the second case (axis) the use of other conjugate linkers would modify the electronic structure (although probably not too much, since the electrons would still find it easy to delocalize along the conjugate stats), but a more detailed investigation is beyond the scope of this article. More recently, a π-conjugated porphyrin nanotube was synthesized, and it was observed that additionally stacking two (*c*-P6) nanorings forms a tube (labeled *t*-P12), which clearly transforms the optical properties due to an increase of the conjugation, followed by metalation with zinc [11]. The increase of conjugation affects the optical properties because when the porphyrin nanoring structures are coupled strongly, leading to conjugate states all over the circumference, light of different frequency can be absorbed on delocalized excited states over the entire circumference, similar to a regular π-system, instead of more localized states located on each porphyrin unit. Recent DFT-calculations have also shown details of the electronic properties in porphyrin nanotubes and, in particular, it was observed abnormal and highly oscillatory bandgaps of these structures by increasing their size [11]. Moving one step beyond, the use of porphyrin tubes in nanodevices faces currently great challenges, not only in their design and fabrication, but also in controlling their structural and functional properties. Notice as well that the use of porphyrins in structures like nanotubes make them easier to handle and connect to terminals, compared to other structures such as single molecules and combinations of them. Also, the use of nanotube structures increases their tunability by introducing factors such as the chirality and the diameter of the nanotube and by making easier to use other methods such as chemical doping [12] , which adds more freedom to the design of specific thermoelectric materials based on porphyrins. Regarding thermoelectric properties, the consideration of p-type materials, like carbon nanotube-based thermoelectric devices, has remarkably increased in recent years [13-18]. The specific use of porphyrins in novel structures changes their electronic properties and can lead, as we will see, to sharp features in the electronic structure around the Fermi level; such features are different from those observed in other porphyrin systems (such as e.g. resonances in single molecule systems), leading to rather different thermoelectric performances (higher performances, in many cases). This is then the first study of the thermoelectric performance of such structures.

The route to convert waste heat into electric power is through thermoelectric materials specifically designed for that [19-22]. The waste heat can be harnessed in different ways and through different devices, including thermal sensors [23-25], aerospace [26, 27] and energy conversion devices [28-31]. In particular, through the Seebeck effect it is possible to generates electricity from sources of waste heat, which is represented by the thermopower coefficient $S = -\Delta V/\Delta T$, where ΔV is the voltage difference generated across a device from a temperature difference ΔT. The efficiency of a thermoelectric converter is defined in terms of the dimensionless figure of

View Article Online
DOI: 10.1039/D4TA08282F

merit $ZT = S^2GT/k$, where G is the electrical conductance (which represents the conduction an electric current across a device) and k is the thermal conductance (which represents the conduction of heat across a device). The aim is to design devices with ZT as high as possible, but finding strategies for minimizing the denominator (k) and maximizing the numerator (S and G) of ZT is currently a big challenge. New alternatives have then to be explored, such as the use of organic materials, whose thermoelectricity has been extensively studied in the last years. For instance, it was measured the room-temperature thermopower *S* of semiconducting single-walled carbon nanotubes (SWCNTs) (160-170 μVK^{-1}) [32], the thermopower (~70 μVK^{-1}) and figure of merit (~0.11 at 305 K) of p-type metallic SWCNTs films [33] and the thermopower of metalloporphyrin/SWCNTs complex composite films ($47\mu VK^{-1}$) [33].

In this paper, we examine the potential of metalloporphyrin nanotubes for thermoelectric performance. The proposed structures, shown in Figure 1 are made of a one-dimensional supercell of hollow-metalloporphyrin nanotubes with three types of transition metal-centers (Zn, Fe, and Fe-Cl; in this last case a Cl atom is bonded to the Fe atom in the center of each molecule; notice we use Cl because this is a halogen atom that leads to precise oxidation/reduction changes between Fe(II)/Fe(III), i.e. to the absorption of one electron, see [34]. In such structures, the hollow-metalloporphyrin nanotube, which has a length L = 6.7 nm and a diameter D = 2.7 nm, is made of butadiyne-linked porphyrin nanorings. Different views of the calculated geometries are also shown in Figure S1 of SI. The coupled states of these nanorings makes the electrons to highly delocalize between them [35]. Such particular electronic structure leads to a wide range of optoelectronic performances [9] and can also be exploited to make electronic and thermoelectric devices. In particular, to exploit the potential of these periodic structures as thermoelectric converters, it is necessary to find asymmetric step-function and narrow delta-function like features in the electronic structure that can lead to large thermoelectric performance [36-39], as we shall see. In order to understand and clarify the role of such features in the thermoelectric performance we present a discussion in the SI information.

View Article Online
DOI: 10.1039/D4TA08282F

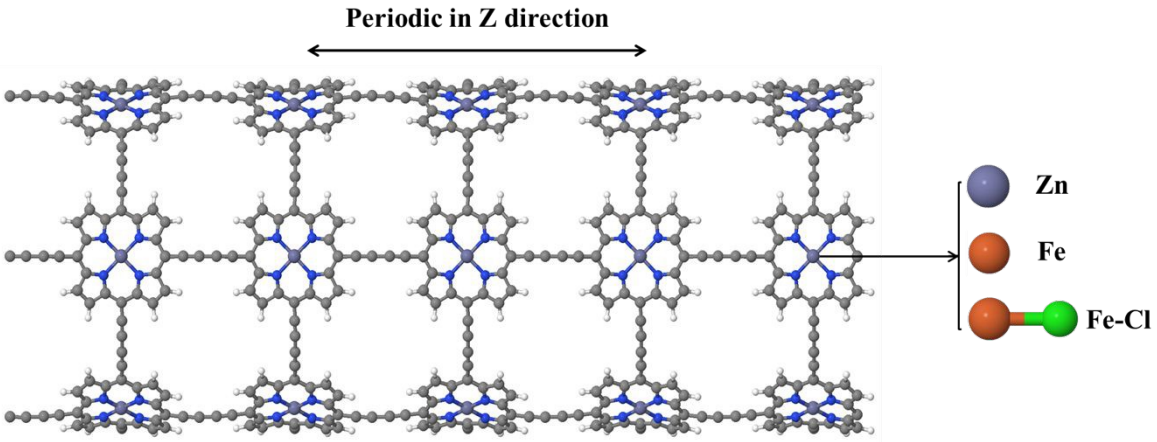

Figure 1. The relaxed supercell of a 30-hollow metalloporphyrin nanotube made of 1,260 atoms. Three possible structures correspond to three metallic atoms (Zn, Fe, and Fe-Cl), which are varied for each structure.

2. Computational Method

We used density functional theory (DFT) as implemented in the SIESTA code [40]. We employed the generalized gradient approximation (GGA-PBE) as exchange and correlation functional [41], double-zeta polarized basis sets to span the valence states and norm-conserving pseudoatomic orbitals to get rid of the core electrons. Notice that a better description of the d states of Fe would still be possible by using DFT+U, since the strong on-site Coulomb repulsion would substantially affect the electronic interactions in the localized d-orbitals. All results were also calculated with such correction, with a U of 4.5 eV. A similar effect would also be produced by more sophisticated functionals, like HSE06, which would open the band gap, but we found that in these cases the results were quantitatively and qualitatively very similar, so we decided not to include it. Notice as well that the use of functionals with dispersion corrections would not be necessary in this case, since no Van der Waals interactions are considered in single nanotubes. We defined the real-space grid with a plane-wave cut-off of 200 Ry and relaxed all geometries until all atomic forces were smaller than 0.02 eV $Å^{-1}$. We also used the GOLLUM quantum transport code [42] to calculate the transmission $T(E)$ and the corresponding thermoelectric coefficients from the electronic structure provided by SIESTA.

View Article Online
DOI: 10.1039/D4TA08282F

3. Results and Discussion

3.1. DFT calculations

Five nanorings units with six metallo-porphyrin were stacked to form the nanotube. We also considered different metallic atoms (Zn, Fe, and Fe-Cl) as central atoms in the metallo-porphyrins. For all these cases, the structures are completely relaxed leading to the nanotubes shown in Figure 1 (different views of the calculated geometries are shown in Figure S1 of the SI). The relaxations are carried out without problem and the nanotubes always relax to the same structure, which shows they are stable (also confirmed by experiments) [6]. Notice that in some cases (PFe and PFe-Cl) there is some deviation from planarity. This deviation is real, as already found for other molecules [43] and not an artifact of the simulations.

Figures S2-S4 of SI show the frontier molecular orbitals (FMOs) of the of PZn, PFe, and PFe-Cl nanorings, respectively. Red corresponds to the positive and blue to negative regions of the wave function. The plots show that the HOMO of PZn ring are distributed through the pathways of π-system, while for the LUMO, are delocalized across their pyrrole subunits.

The butadiyne linkers (C4) between the 6-porphyrin nanoring have frontier orbitals in antiphase, which is similar that of the 12-porphyrin nanotube [6, 44]. However, the FMOs are distributed through the pyrrole subunits of porphyrins with scarcity around the metal-centers Fe(II) and significant reduction across the C4-linkers of the PFe(II) nanoring.

For the PFe(III) complexed with a Cl−, the HOMO is often distributed cross π-system and the C4-linkers, whereas the LUMO is partially distributed and the FMOs resembles that of the C4-linkers in PFe(II) nanoring. Notice that the donation of electrons from the HOMO PFe populates the counter ion Cl, while for the LUMO of PFe-Cl, there are two bared chloride atoms.

For each unit cell of the metallo-porphyrin nanoring structure in Figure 2 (right-hand panels), the electronic band structure (left-hand panels) and density of state (DOS) (central panels) were calculated. The calculations show that the PZn nanoring structure has in its electronic structure an energy gap of ∼1 eV at the Fermi energy. The bandgap appears for this particular size (6 porphyrin units around the tube) [11]. For the metal-center with Fe, however, panel *(b)* shows that the energy gap moves below the Fermi energy E_F, which makes this nanotube metallic. Finally, for the PFe(III)- complex, which has the presence of Cl^- counter anions that capture electrons,

View Article Online
DOI: 10.1039/D4TA08282F

the energy gap shifts above the E_F and makes it also metallic, as shown in panel *(c)*. Notice as well that the gap is always direct, since the top of the valence band coincides with the bottom of the conduction band.

For each metalloporphyrin nanotube (PZn, PFe and PFe-Cl) in Figure 2, the transmission $T(E)$ was calculated, as can be seen in Figure 3. Since these structures are periodic, $T(E)$ in all these cases is equal to number of open channels and is given by a series of step functions. Figure 3 *(a)*, show that porphyrin nanotube with Zn atoms an asymmetric step-function in the transmission $T(E)$ appears around Fermi energy, while for the nanotube with Fe atoms a series of steps related to bands of the metal atom and the molecule appear. Finally, for the PFe nanotube in presence of a Cl^- counter anions, a broad and asymmetric structure forms around the Fermi level. Notice that, in particular, steps near the Fermi level are likely to lead to large thermoelectric performances. It is then convenient to study how the thermoelectric coefficients change with the position of Fermi energy E_F relative to the original one E_F^{DFT}. This can be achieved experimentally, by using electrostatic or electrochemical environments or by doping, i.e. by varying for instance the transition metal in the center of the porphyrin.

View Article Online
DOI: 10.1039/D4TA08282F

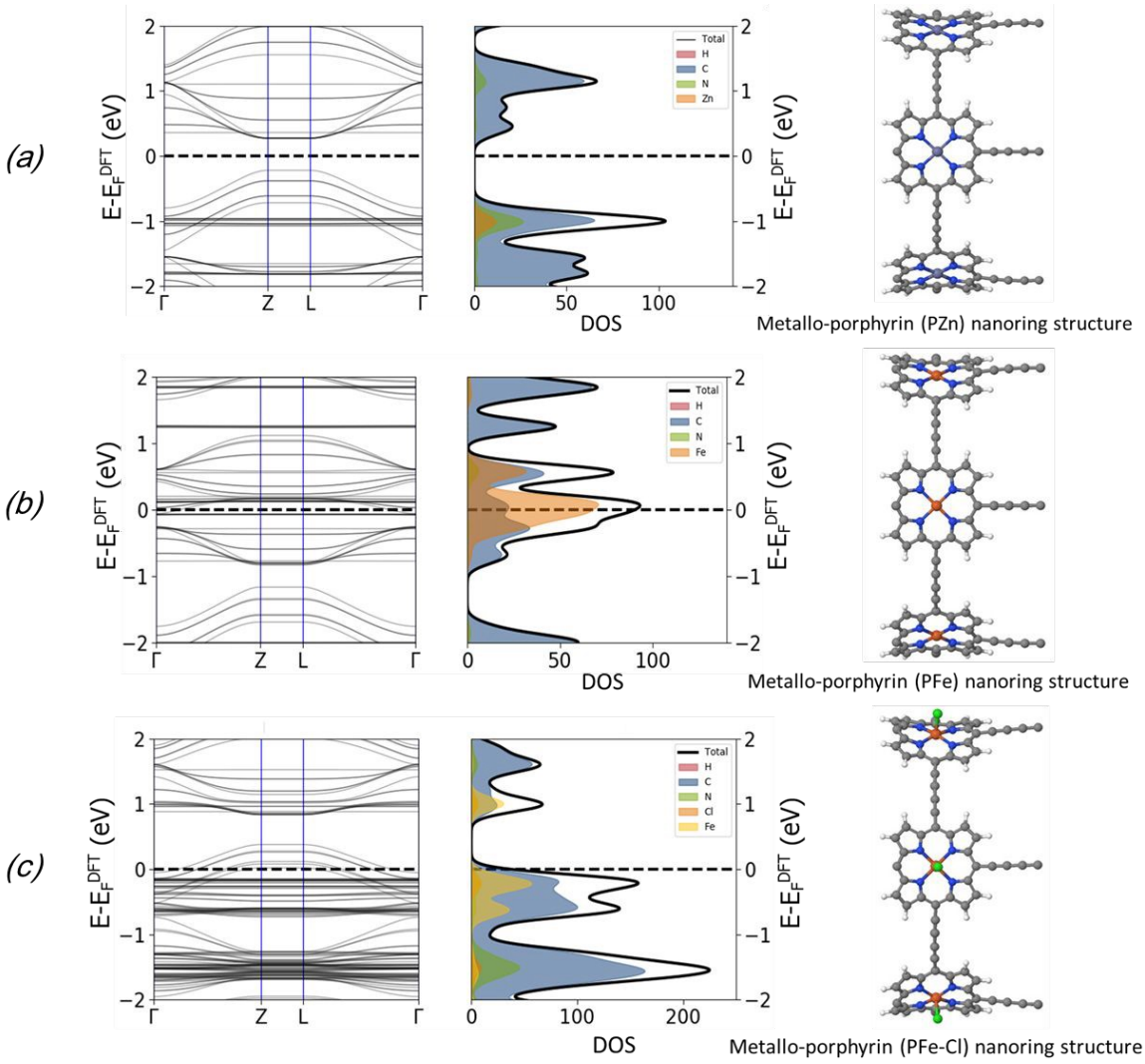

Figure 2. *(a)-(c)* right, the DFT calculated optimized geometry of the unit cell for 6-metallo-porphyrin nanoring structures with different metallic atoms (Zn, Fe, and Fe-Cl), *(a)-(c)* middle, the density of states (DOS) and *(a)-(c)* left, the band structure for all structures, respectively. The dashed lines indicate the Fermi level.

Once the transmission coefficient $T(E)$ is obtained, then the room-temperature electrical conductances (pink dotted curves in the left-hand panels of Figure 3 and the thermoelectric coefficients (panel *(b)* in Figure 3) can be calculated using Equations (S3) to (S6) in the SI. The variation of the conductance, both electrical and thermal, is easy to understand by looking at the transmission, since this quantity roughly follows it. The thermopower follows the derivative, so it reaches high values when there are sharp variations of the transmission. In particular, if the Fermi level is on the right (left) of a sharp feature the thermopower is positive (negative). Notice as well that the transmission for all these systems has in general peaks close to the Fermi level, as opposed to typical carbon nanotubes, which have a gap or a flat transmission around it (giving poorer

View Article Online
DOI: 10.1039/D4TA08282F

thermoelectric performances). Figures 3 also shows the power factor ($PF = \sigma^2 S$) in panel *(d)*, and the electronic figure of merit ZT_e in panel *(f)* over a arrange of Fermi energies. The calculations show that for the PZn nanotube, the asymmetric-located feature in $T(E)$ around the Fermi level leads to the highest positive and negative magnitudes of the thermopowers: $S = +760$ μV/K at $E_F - E_F^{DFT} = 0$ eV and $S = -1065$ μV/K at $E_F - E_F^{DFT} = 0.07$ eV. The explanation for such high values is that the Fermi energy after p-doping (metal into porphyrin) at the PZn lies near to HOMO, so that the metal causes the Fermi energy to sit closer to the HOMO, in a region of a steep slope for the transmission function. This behaviour is shown in Figure 3 *(a)*, where the Zn atom causes the energy levels of the porphyrin nanotube to increase in energy and therefore the HOMO resonance moves closer to the Fermi energy, leading to an increase in the slope and hence to a more negative Seebeck coefficient. Whereas in the case of PFe, the step-function remarkably decreases (around -0.2 eV) accompanied with broad delta-function (~ 0.6 eV) moving away from DFT-Fermi energy leading to decrease in the slope and this produces low thermopower at $E_F = E_F^{DFT}$. For porphyrin nanotubes with Fe-Cl, the step-function shifts away from Fermi energy to the higher energies and the broad delta function emerges over a range of Fermi energies resulting to decrease in the slope and this produces also low thermopower. For porphyrin nanotubes with Fe and Fe-Cl, *S* takes values of -52 and +1.7 μV/K at $E_F = E_F^{DFT}$, respectively. As before, both the magnitude and sign of thermopower depend on the location of Fermi energy and rather high values can appear for certain E_F. For instance, for the nanotube with Fe atoms the thermopower is -285 μV/K at $E_F - E_F^{DFT} = -0.2$ eV, while for the nanotube with Fe-Cl, it can reach +628 μV/K at $E_F - E_F^{DFT} = 0.58$ eV and -770 μV/K at $E_F - E_F^{DFT} = 0.67$ eV. These values are much higher than those typically found in molecular electronics systems or similar systems such as nanowires of molecules [45, 46], or other systems made of periodic arrays of nanoscale elements [47]. Such high values of thermopower would allow the fabrication of much more efficient heat-to-electricity converters, coolers and other systems with applications in several industries, ranging from domestic systems to the car or aerospace industries.

Regarding the figure of merit, the porphyrin nanotube in the presence of Zn has the highest value of ZT_e (around 100), which reflects the high values of the thermopower and conductance. Such high values make PZn nanotube of a favourable materials for thermoelectric devices. Notice as well that for bulk systems, the figure of merit $ZT = S^2\sigma T/k$ involves two crucial quantities, which are power factor ($PF = S^2\sigma$) and the total thermal conductivity (k), where k includes both electron and phonon contributions (this differs from $ZT_e = S^2\sigma T/k_e$ where k_e has only contributions from electrons). The quantity $PF = S^2\sigma$, the power factor, can also be calculated to have an idea of its contribution to *ZT*. The conductivity is $\sigma = GL/A$, where L is the length of

View Article Online
DOI: 10.1039/D4TA08282F

molecular device and A is the cross-sectional area. In this work we use $L = 6.7$ nm and $A = 7.4$ nm^2. These values come from the length and cross-section used in the simulations. Above that length the nanotube is assumed to be connected to seamlessly to metallic electrodes. The results show that the highest power factor is obtained at $E_F - E_F^{DFT} = 0.35$ eV ($PF = 8 \times 10^{-3}$ W/m K^2) in case of the PZn nanotube. For PFe, the power factor is 7×10^{-3} $W/m.K^2$ at $E_F - E_F^{DFT} = -0.25$ eV. A similar value is found at $E_F - E_F^{DFT} = 0.86$ eV for the PFe nanotube in the presence of a Cl^- counter anion. These values are higher than the measured value of the single-walled carbon nanotube/ZnTPP, which was found to be 247×10^{-6} $W/m.K^2$[33].

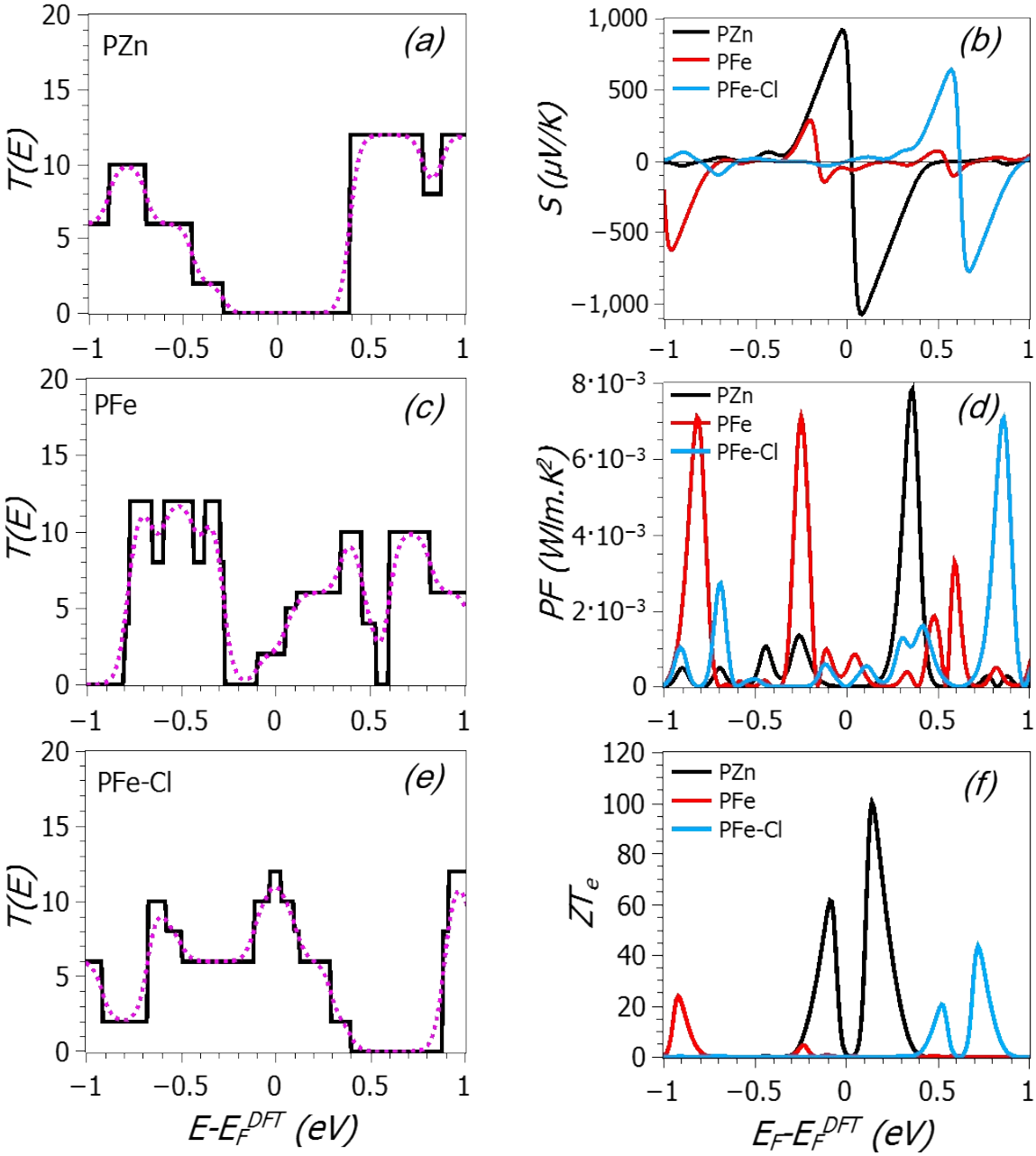

View Article Online
DOI: 10.1039/D4TA08282F

Figure 3. For the metallo-porphyrin nanotube structures of Figure 1, the black solid line in each panel shows the calculated transmission coefficient $T(E)$ versus energy for *(a)* PZn, (c) PFe *(e)* PFe-Cl. The pink dotted curves show the room-temperature electrical conductance. Figure 3 *(b)*, *(d)* and *(f)* show the thermopower S, power factor $PF = \sigma S^2$ and electronic figure of merit ZT_e over a range of Fermi energies.

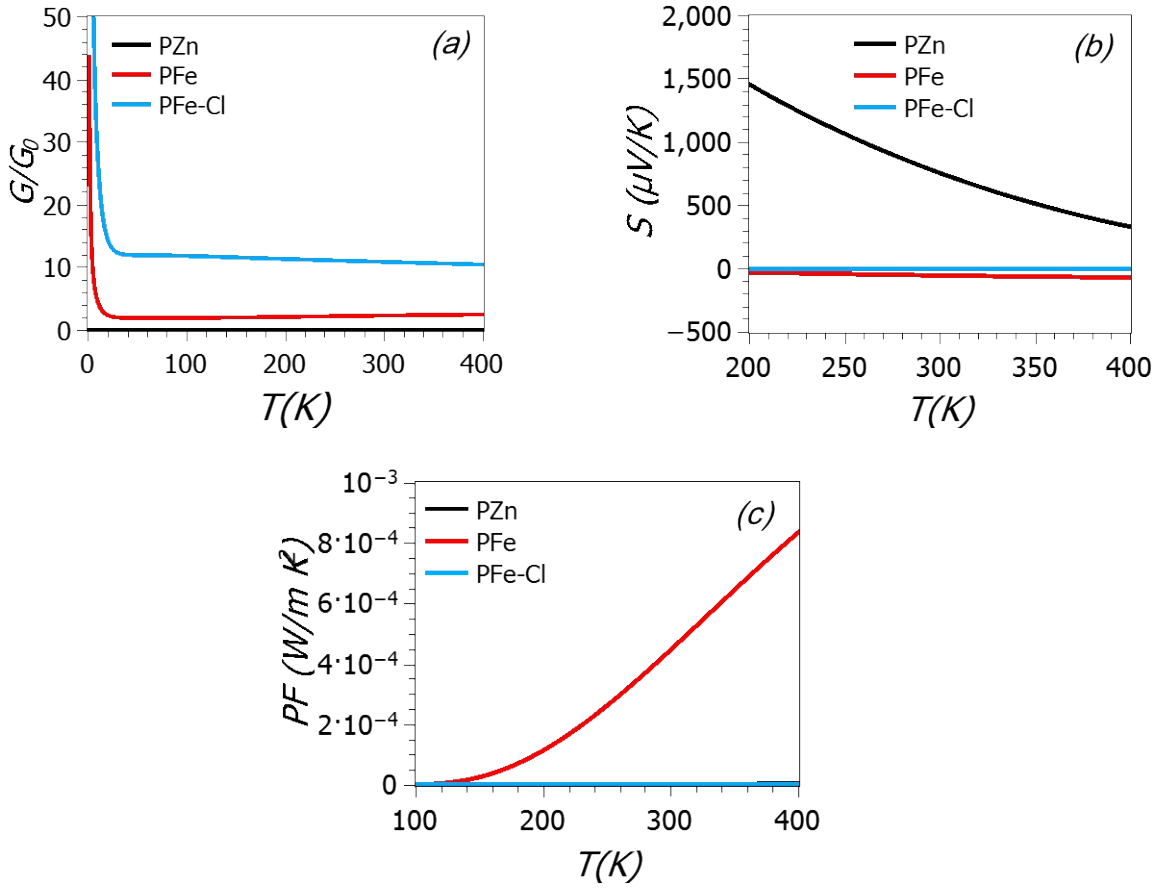

Figure 4. Eelectrical conductance G (a), thermopower S (b) and power factor $PF = \sigma S^2$ (c) as a function of temperature T, evaluated at at $E_F - E_F^{DFT} = 0$ eV.

View Article Online
DOI: 10.1039/D4TA08282F

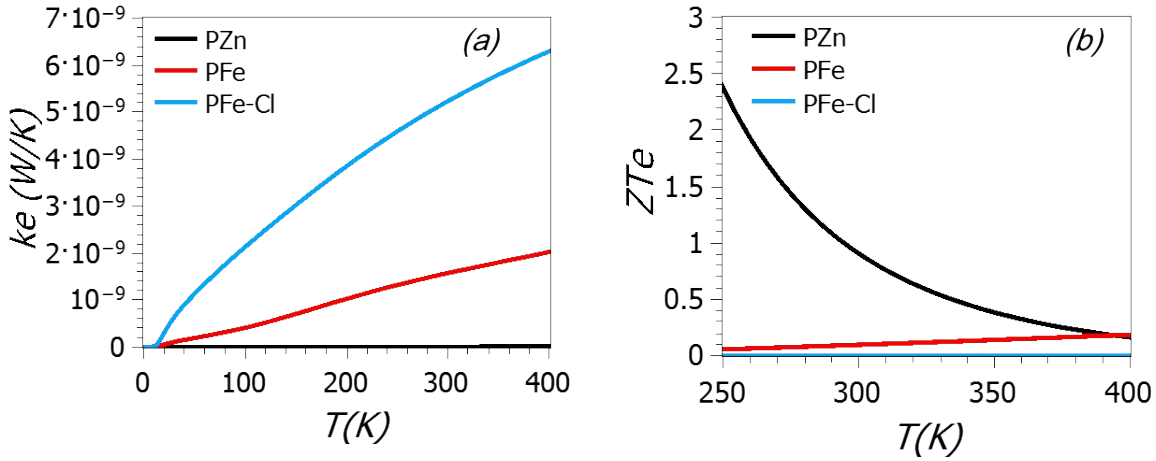

Figure 5. Electronic contribution to the thermal conductance (k_e) (a) and figure of merit ZT_e (b) over a range of temperatures T.

Finally, the temperature dependence of the thermoelectric coefficients was also calculated. The electrical conductance G, thermopower S and power factor $PF = \sigma S^2$ are shown over a range of temperature T and evaluated at the DFT-Fermi energy in Figure 4*(a)-(c)*. As can be seen, the electrical conductance strongly decreases as the temperature increases, which is a consequence of the temperature window covering larger portions with small conductance as it increases (i.e. as the derivative of the Fermi distribution becomes wider). The thermopower has a similar trend for PZn, although the decrease is smaller and sustained, while it is roughly constant or decreases (it becomes more negative) a little for the other two cases; the decrease or increase of this quantity depends on the entering of more sharp features in the temperature window. Finally, the power factor decreases for all cases but for the PFe system, where it increases due mainly to the increase of the absolute value of the thermopower in this case. Also, the electronic contribution to the thermal conductance (k_e) and figure of merit ZT_e as a function of temperature T are shown in Figure 5 *(a)* and *(b)*. The electronic thermal conductance of PFe-Cl and PFe nanotubes increases with temperature due to the covering of the temperature window of more features as it increases, while the highest temperature-dependent figure of merit, which is a combination of all previous quantities, occurs for the PZn nanotube, with the highest values given at high temperatures ($> 300\ K$).

3.2. DFT+U calculations

To describe accurately the electronic properties in porphyrin nanoring, the DFT-density of states (DOS) calculation for the PFe and PFe-Cl rings were carried out using GGA-PBE, GGA+*U* and the hybrid functional GGA- HSE06. The results of the HSE06 calculation are similar to those of GGA for PFe around the DFT-Fermi energy, while the largest differences are observed with GGA+*U*, (as shown in Figures S5 and S6 in the SI).

View Article Online
DOI: 10.1039/D4TA08282F

Comparing GGA and HSE06, we found that HSE06 changed the size of the energy gaps of the PFe and PFe-Cl rings. For the PFe ring, the PBE band gap is located below the DFT-Fermi energy, as shown in Figure 2(*b*), and has a value of 0.8 eV, whereas the HSE06 energy gap reduces it to approximately 0.2 eV, as shown in Figure S5(*c*). In case of the PFe-Cl ring, the PBE band gap lies above the Fermi energy roughly 0.75 eV (Figure 2(*c*)), while with HSE06 it disappears and a new energy gap below the Fermi energy appears with a value of ~0.1 eV, as shown in Figure S6(*c*).

Using DFT+U combined with Green's function formalism, the transmission *T(E)* was calculated for periodic structures PFe and PFe-Cl nanotubes. The calculation shows that the steps-functions like *T(E)*s were shifted about 0.2 eV near to DFT-Fermi energy for the PFe nanotube as shown in Figure 6 *(a)*, while for the PFe-Cl, it can be seen in Figure 6 *(b)* a higher broad asymmetric delta-function (ranges about 1.6 eV) than those in PFe (ranges about 0.6 eV) around the Fermi energy.

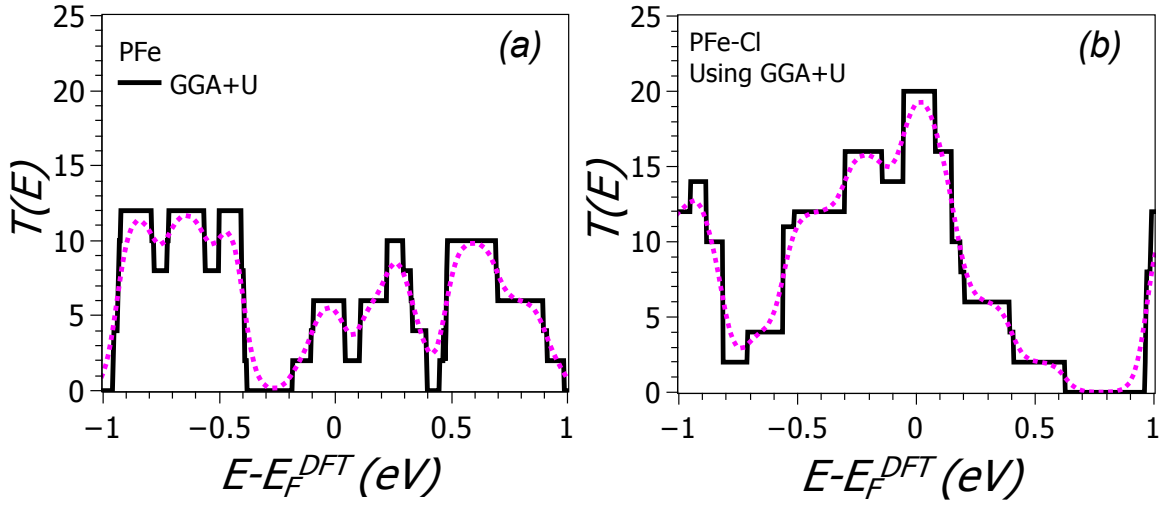

Figure 6. The black solid line shows the DFT+U calculation of transmission coefficient *T*(*E*) versus energy for the metallo-porphyrin nanotube structures *(a)* PFe and *(b)* PFe-Cl. The pink dotted curve shows the room-temperature electrical conductance.

This particular feature (steps near E_F) is favorable for enhance the thermoelectric properties and again from transmission *T(E)* based GGA+U functional the thermoelectric coefficients were calculated, shown in Figures 7 *(a)-(d)*. The higher room-temperature thermopower *S* and power factor *PF* were observed for PFe nanotube at $E_F - E_F^{DFT} = -3.4$ eV (near the step-function) by the values $+262\ \mu V/K$ and $6.3 \times 10^{-3}\ W/m.K^2$, respectively. The higher values of those are accompanied with lower electronic thermal conductance $k_e =$

View Article Online
DOI: 10.1039/D4TA08282F

3.5×10^{-10} W/K results the higher electronic figure of merit $ZT_e = 6.2$. Whereas for the PFe in the presence of counter ion Cl^-, the higher thermoelectric coefficient appears within the range of Fermi energies $E_F - E_F^{DFT}$ from 0.8 to 0.94 eV, which lies near the step-function of transmission. This leads to change the sign and magnitude of thermopower $S = -487$ μV/K , increases the value of power factor 7.5×10^{-3} W/m.K^2 and enhance the electronic figure of merit to $ZT_e = 18$. This ability to enhance the thermoelectric coefficients of metalloporphyrin nanotube depends on consideration of full efficiency figure of merit ZT by taking into account total thermal conductance ($\kappa = \kappa_e + \kappa_{ph}$), where κ_{ph} is the phonon thermal conductance and $ZT = \sigma S^2 T/k$. Therefore, to find the full efficiency ZT, the κ_{ph} value needs to be considered. The comparison between GGA and GGA+U calculations are found in Figures (S13-S20) of the SI.

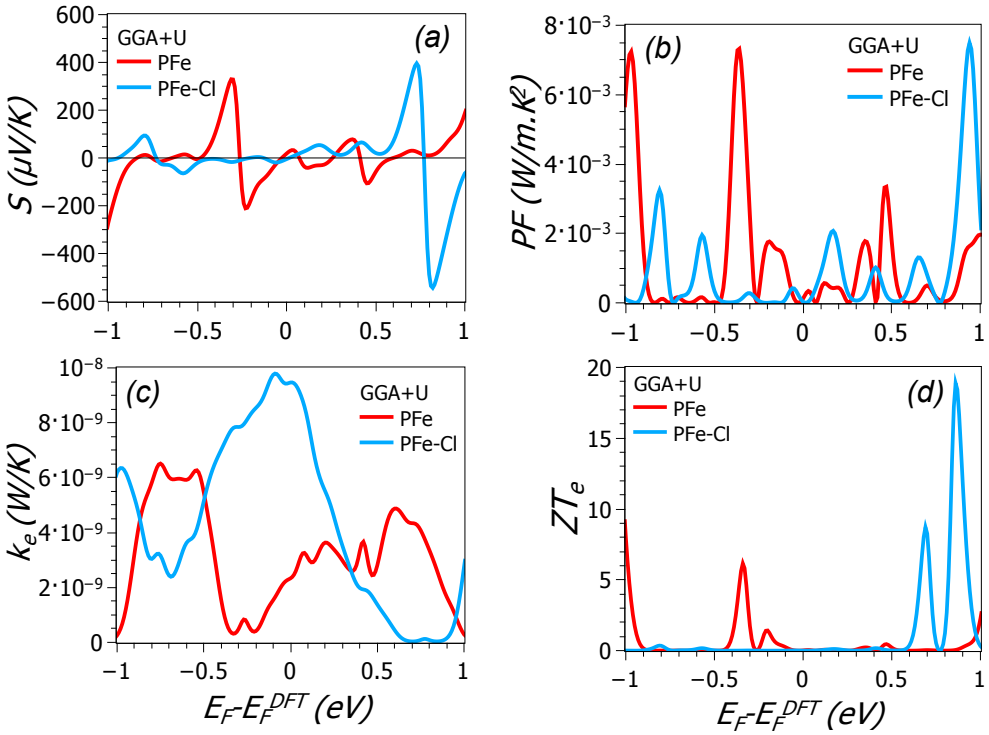

Figure 7. The room-temperature thermoelectric coefficients calculation using DFT+U for the PFe and PFe-Cl nanotubes, where *(a)* thermopower *S*, *(b)* power-factor $PF = \sigma S^2$, *(c)* electronic thermal conductance k_e and *(d)* electronic figure of merit ZT_e versus Fermi energy.

4. Conclusions

We have demonstrated the possibility to design metalloporphyrin nanotube thermoelectric devices with particular electronic properties such as specific band gap values and band structures by varying the central

View Article Online
DOI: 10.1039/D4TA08282F

metallic atom of the porphyrin unit and the type of self-assembly formations (nanotubes, in this case). These variations can highly affect the transmission and therefore tune the thermoelectric properties. Our aim was to examine three cases of metalloporphyrin nanotubes (PZn, PFe, and PFe-Cl), with induced asymmetric step-functions around the Fermi level in the transmission coefficients. Finding such features can significantly improve the thermoelectric performance.

The GGA calculations show that an asymmetric-located features in the transmission lead to rather high positive or negative values of the thermopower for many values of $E_{\mathrm{F}} - E_{\mathrm{F}}^{\mathrm{DFT}}$. The PZn nanotube exhibited the best thermoelectric performance with a rather high room-temperature thermopower of $S = +760\ \mu V/K$ at the DFT-Fermi energy. The thermopower can also switch sign to negative, with the highest negative magnitude of $S = -1065\ \mu V/K$ at $E_{\mathrm{F}} - E_{\mathrm{F}}^{\mathrm{DFT}} = 0.07$ eV. Notice that the sign of the thermopower depends on the type of feature that is at the Fermi level; if such feature has a "positive slope" (i.e. the feature is below the Fermi level) the thermopower is negative, while it is positive in the opposite case. Since the Fermi level scan can cover both types of features the thermopower switch sign in various cases. The resulting PFe and PFe-Cl thermopowers range from +628 μV/K at $E_{\mathrm{F}} - E_{\mathrm{F}}^{\mathrm{DFT}} = 0.58$ eV to -770 μV/K at $E_{\mathrm{F}} - E_{\mathrm{F}}^{\mathrm{DFT}} = 0.67$ eV. On the other hand, the highest power factor, $8 \times 10^{-3}\ \frac{\mathrm{W}}{\mathrm{m}}.\ \mathrm{K}^2$, was found for the PZn nanotube at $E_{\mathrm{F}} - E_{\mathrm{F}}^{\mathrm{DFT}} = 0.35$ eV, which is much higher than the measured value of single-walled carbon nanotube/ZnTPP composites ($247 \times 10^{-6}\ \mathrm{W/m.\ K^2}$), improving therefore the thermoelectric properties of such systems and the degree of miniaturization over mixtures of different nanoscale elements [33]. Finally, the porphyrin nanotube with Zn has the highest value of ZT_{e}, much higher than other nanoscale systems. All these rather high thermoelectric coefficients make these nanotubes favourable materials for thermoelectric conversion, with ppromising performances for thermoelectric applications.

For the GGA+*U* calculations, particular features near the Fermi level enhances the thermoelectric properties giving rise to higher room-temperature thermopower *S* and power factor *PF* for PFe nanotubes at $E_F - E_F^{DFT} = -3.4$ eV (near the step-function), with values $+262$ μV/K and 6.3×10^{-3} W/m.K^2, respectively. Something similar is found for the thermal conductance, $k_e = 3.5 \times 10^{-10}$ W/K, and the electronic figure of merit $ZT_e = 6.2$. Whereas for the PFe-Cl, the higher thermoelectric coefficients occurs within the range of Fermi energies $E_F - E_F^{DFT}$ from 0.8 to 0.94 e, near the step-function of transmission. This leads to a change in the sign and magnitude of thermpower $S = -487$ μV/K and increases the value of power factor

View Article Online
DOI: 10.1039/D4TA08282F

7.5×10^{-3} W/m.K^2 increasing as well figure of merit to $ZT_e = 18$. This shows that the inclusion of U is necessary in this case, as it leads to different results (higher thermoelectric performances).

Declaration of Competing Interest

The authors declare no conflict of interest.

Acknowledgements

Qusiy H. Al-Galiby and Laith A. Algharagholy acknowledge the Iraqi Ministry of Higher Education and Scientific Research, University of Al-Qadisiyah and University of Sumer for the support. Hatef Sadeghi acknowledges the UKRI for Future Leaders Fellowship number MR/S015329/2 and MR/X015181/1. V. M. García-Suárez thanks the European Union and the Spanish Ministry of Science, Innovation and Universities for funding through the project MCINN-24-PCI2024-153437.

Author contributions

Qusiy H. Al-Galiby, Laith A. Algharagholy, Hatef Sadeghi and V. M. García-Suárez were involved in interpreting the results, writing and commenting the manuscript.

Data Availability Statement

The data that support the findings of this study are available from the corresponding author upon reasonable request.

ORCID:

Qusiy H. Al-Galiby: 0009-0004-6691-5868

Laith A. Algharagholy: 0000-0002-0411-879X

Sadeghi, Hatef: 0000-0001-5398-8620

García-Suárez, Víctor: 0000-0002-7392-4648

References

1. Wang, Z., C.J. Medforth, and J.A. Shelnutt, *Self-metallization of photocatalytic porphyrin nanotubes.* Journal of the American Chemical Society, 2004. **126**(51): p. 16720-16721.
2. Wang, Z., C.J. Medforth, and J.A. Shelnutt, *Porphyrin nanotubes by ionic self-assembly.* Journal of the American Chemical Society, 2004. **126**(49): p. 15954-15955.
3. Vlaming, S., et al., *Exciton spectra and the microscopic structure of self-assembled porphyrin nanotubes.* The journal of physical chemistry B, 2009. **113**(8): p. 2273-2283.

View Article Online
DOI: 10.1039/D4TA08282F

4. Zhao, Q., et al., *Out-of-plane coordinated porphyrin nanotubes with enhanced singlet oxygen generation efficiency.* Scientific Reports, 2016. **6**(1): p. 31339.
5. Zhu, G., et al., *Curvature-dependent selectivity of CO2 electrocatalytic reduction on cobalt porphyrin nanotubes.* ACS Catalysis, 2016. **6**(9): p. 6294-6301.
6. Haver, R. and H.L. Anderson, *Synthesis and properties of porphyrin nanotubes.* Helvetica Chimica Acta, 2019. **102**(1): p. e1800211.
7. Idrees, S., et al., *Porphyrin nanotubes based on a hydrogen-bonded organic framework.* Nanoscale, 2022. **14**(39): p. 14630-14635.
8. Posligua, V., et al., *Band structures of periodic porphyrin nanostructures.* The Journal of Physical Chemistry C, 2018. **122**(41): p. 23790-23798.
9. Franco, R., et al., *Molecular organization in self-assembled binary porphyrin nanotubes revealed by resonance Raman spectroscopy.* Physical Chemistry Chemical Physics, 2010. **12**(16): p. 4072-4077.
10. Hoffmann, M., et al., *Enhanced p conjugation around a porphyrin [6] nanoring.* ANGEWANDTE CHEMIE-INTERNATIONAL EDITION IN ENGLISH-, 2008. **47**(27): p. 4993.
11. Allec, S.I., N.V. Ilawe, and B.M. Wong, *Unusual bandgap oscillations in template-directed π-conjugated porphyrin nanotubes.* The Journal of Physical Chemistry Letters, 2016. **7**(13): p. 2362-2367.
12. Nishinaka, M., et al., *n-Type Carbon Nanotubes Doped by Cross-Linked Organic Superbase for Stable Thermoelectric Materials.* Energy Material Advances, 2024. **5**: p. 0123.
13. Blackburn, J.L., et al., *Carbon-nanotube-based thermoelectric materials and devices.* Advanced Materials, 2018. **30**(11): p. 1704386.
14. Meng, C., C. Liu, and S. Fan, *A promising approach to enhanced thermoelectric properties using carbon nanotube networks.* Advanced Materials, 2010. **22**(4): p. 535-539.
15. Avery, A.D., et al., *Tailored semiconducting carbon nanotube networks with enhanced thermoelectric properties.* Nature Energy, 2016. **1**(4): p. 1-9.
16. Jin, Q., et al., *Flexible layer-structured Bi2Te3 thermoelectric on a carbon nanotube scaffold.* Nature materials, 2019. **18**(1): p. 62-68.
17. Ren, F., et al., *Thermoelectric and mechanical properties of multi-walled carbon nanotube doped Bi0. 4Sb1. 6Te3 thermoelectric material.* Applied Physics Letters, 2013. **103**(22).
18. Zhou, W., et al., *High-performance and compact-designed flexible thermoelectric modules enabled by a reticulate carbon nanotube architecture.* Nature communications, 2017. **8**(1): p. 14886.
19. Bell, L.E., *Cooling, heating, generating power, and recovering waste heat with thermoelectric systems.* science, 2008. **321**(5895): p. 1457-1461.
20. Garofalo, E., et al., *Waste heat to power: Technologies, current applications, and future potential.* Energy Technology, 2020. **8**(11): p. 2000413.
21. Jouhara, H., et al., *Waste heat recovery technologies and applications.* Thermal Science and Engineering Progress, 2018. **6**: p. 268-289.
22. Chiolerio, A., et al., *Waste heat to power conversion by means of thermomagnetic hydrodynamic energy harvester.* Applied Energy, 2020. **277**: p. 115591.
23. Van Herwaarden, A. and P. Sarro, *Thermal sensors based on the Seebeck effect.* Sensors and Actuators, 1986. **10**(3-4): p. 321-346.
24. Kirihara, A., et al., *Flexible heat-flow sensing sheets based on the longitudinal spin Seebeck effect using one-dimensional spin-current conducting films.* Scientific reports, 2016. **6**(1): p. 23114.
25. Zhao, Y., et al., *Ultrasensitive Photothermal Spectroscopy: Harnessing the Seebeck Effect for Attogram-Level Detection.* Nano Letters, 2023. **23**(17): p. 7883-7889.
26. Boccardi, S., F. Ciampa, and M. Meo, *Design and development of a heatsink for thermo-electric power harvesting in aerospace applications.* Smart Materials and Structures, 2019. **28**(10): p. 105057.

View Article Online
DOI: 10.1039/D4TA08282F

27. Sarris, A., B. Bhatti, and F. Ciampa, *Thermoelectric energy harvesting using vapour chamber coolers for aerospace applications.* Journal of Intelligent Material Systems and Structures, 2022. **33**(12): p. 1602-1612.
28. Arico, A.S., et al., *Nanostructured materials for advanced energy conversion and storage devices.* Nature materials, 2005. **4**(5): p. 366-377.
29. Cullen, J.M. and J.M. Allwood, *Theoretical efficiency limits for energy conversion devices.* Energy, 2010. **35**(5): p. 2059-2069.
30. Huang, L., et al., *Fiber-based energy conversion devices for human-body energy harvesting.* Advanced Materials, 2020. **32**(5): p. 1902034.
31. Li, W., J. Liu, and D. Zhao, *Mesoporous materials for energy conversion and storage devices.* Nature Reviews Materials, 2016. **1**(6): p. 1-17.
32. Nakai, Y., et al., *Giant Seebeck coefficient in semiconducting single-wall carbon nanotube film.* Applied Physics Express, 2014. **7**(2): p. 025103.
33. Zhou, Y., et al., *High performance p-type organic thermoelectric materials based on metalloporphyrin/single-walled carbon nanotube composite films.* Journal of Power Sources, 2019. **423**: p. 152-158.
34. Al-Galiby, Q.H., et al., *Tuning the thermoelectric properties of metallo-porphyrins.* Nanoscale, 2016. **8**(4): p. 2428-2433.
35. Rickhaus, M., et al., *Single-acetylene linked porphyrin nanorings.* Journal of the American Chemical Society, 2017. **139**(46): p. 16502-16505.
36. Algharagholy, L.A., et al., *Tuning thermoelectric properties of graphene/boron nitride heterostructures.* Nanotechnology, 2015. **26**(47): p. 475401.
37. Lambert, C.J., H. Sadeghi, and Q.H. Al-Galiby, *Quantum-interference-enhanced thermoelectricity in single molecules and molecular films.* Comptes Rendus Physique, 2016. **17**(10): p. 1084-1095.
38. Sadeghi, H., S. Sangtarash, and C.J. Lambert, *Enhanced thermoelectric efficiency of porous silicene nanoribbons.* Scientific reports, 2015. **5**(1): p. 9514.
39. Sadeghi, H., S. Sangtarash, and C.J. Lambert, *Enhancing the thermoelectric figure of merit in engineered graphene nanoribbons.* Beilstein journal of nanotechnology, 2015. **6**(1): p. 1176-1182.
40. Soler, J.M., et al., *The SIESTA method for ab initio order-N materials simulation.* Journal of Physics: Condensed Matter, 2002. **14**(11): p. 2745.
41. Perdew, J.P., K. Burke, and M. Ernzerhof, *Generalized gradient approximation made simple.* Physical review letters, 1996. **77**(18): p. 3865.
42. Ferrer, J., et al., *GOLLUM: a next-generation simulation tool for electron, thermal and spin transport.* New Journal of Physics, 2014. **16**(9): p. 093029.
43. Al-Galiby, Q., et al., *Exploiting the extended π-system of perylene bisimide for label-free single-molecule sensing.* Journal of Materials Chemistry C, 2015. **3**(9): p. 2101-2106.
44. Neuhaus, P., et al., *A molecular nanotube with three-dimensional π-conjugation.* Angewandte Chemie, 2015. **127**(25): p. 7452-7456.
45. Paulsson, M. and S. Datta, *Thermoelectric effect in molecular electronics.* Physical Review B, 2003. **67**(24): p. 241403.
46. Rincón-García, L., et al., *Thermopower measurements in molecular junctions.* Chemical Society Reviews, 2016. **45**(15): p. 4285-4306.
47. Deb, J., et al., *Thermoelectric properties of pristine graphyne and the BN-doped graphyne family.* ACS omega, 2021. **6**(31): p. 20149-20157.

The data that support the findings of this study are available from the corresponding author upon reasonable request.

View Article Online
DOI: 10.1039/D4TA08282F